NASA Technical Memorandum 105144
AIAA-91-2350

Performance and Optimization of a "Derated" Ion Thruster for Auxiliary Propulsion

Michael J. Patterson
Lewis Research Center
Cleveland, Ohio

and

John E. Foster
Jackson State University
Jackson, Mississippi

Prepared for the
27th Joint Propulsion Meeting
cosponsored by the AIAA, SAE, ASME and ASEE
Sacramento, California, June 24-27, 1991

NASA

AIAA 91-2350

PERFORMANCE AND OPTIMIZATION OF A "DERATED" ION THRUSTER FOR AUXILIARY PROPULSION

Michael J. Patterson
National Aeronautics and Space Administration
Lewis Research Center
Cleveland, Ohio 44135

John E. Foster
Department of Physics and Atmospheric Sciences
Jackson State University
Jackson, Mississippi 39217

This paper discusses the characteristics and implications of use of a derated ion thruster for north-south-stationkeeping (NSSK) propulsion. A derated thruster is a 30 cm diameter primary propulsion ion thruster operated at highly throttled conditions appropriate to NSSK functions. The performance characteristics of a 30 cm ion thruster are presented, emphasizing throttled operation at low specific impulse and high thrust-to-power ratio. Performance data and component erosion are compared to other NSSK ion thrusters. Operations benefits derived from the performance advantages of the derated approach are examined assuming an INTELSAT VII-type spacecraft. Minimum ground test facility pumping capabilities required to maintain facility enhanced accelerator grid erosion at acceptable levels in a lifetest are quantified as a function of thruster operating condition. Novel approaches to reducing the derated thruster mass and volume are also discussed.

Introduction

A number of flight experiments and demonstrations of ion auxiliary propulsion systems are proposed for the decade of the nineties, including the Federal Republic of Germany's RITA-10 system on EURECA-1 and SAT-2[1], the United Kingdom's UK-10 system on SAT-2[2], and the Japanese MELCO system on ETS-VI.[3] All of these stationkeeping ion propulsion systems incorporate the use of relatively small (≤ 13 cm diameter) xenon ion thrusters. As a result of the combined small beam area and the required NSSK thrusting levels, these thrusters generally operate near both thermal and current density design limits, over a small throttling range.

To maximize the beam current, and thereby maximize thrust, these engines operate at high grid extraction voltages, which in turn results in a high specific impulse. The thrust levels of these devices typically result in required total accumulated thrusting times in excess of one year for a 15 year NSSK application. These in-space thrusting times require ground qualification testing for extensive periods of time, ranging from 1.5 to 2 times the on-orbit life.

An alternative approach to the application of ion thrusters for auxiliary propulsion is the "derated" ion thruster. The specific derated ion thruster is defined here as a 30 cm engine developed for primary propulsion, but operated under highly-throttled conditions in the power range typical of auxiliary propulsion thrusters (~0.6-2.0 kW). This derated approach was selected for evaluation as it promises operations and reliability advantages over the conventional smaller thruster approaches to NSSK.

In this paper the operations and reliability impacts of the derated ion thruster are quantified. Experimental data obtained from a 30 cm xenon ion thruster are used as the basis for performance comparisons to the smaller NSSK ion thrusters. Additionally, wear-test data and analyses are used to develop parameters to quantify thruster component erosion and lifetime, enabling a comparison of thruster life expectations.

Apparatus and Procedure

Experiments to characterize performance were conducted using a 30 cm diameter laboratory model ring-cusp ion thruster tested on xenon propellant. This third-

generation design is shown in the cutaway drawing of Fig. 1. The thruster incorporates a segmented-anode geometry, consisting of 3 segments of 0.76 mm thick stainless steel, with an exterior chamber of 0.76 mm thick cold-rolled steel. The laboratory model thruster uses a distributed propellant injection for the main flow.

The thruster uses samarium-cobalt permanent magnets to create a cusped field magnetic boundary in the discharge chamber. The magnets are arranged in rings of alternating polarity along the steel chamber walls, with the return flux carried by the steel. Conventional hollow cathodes are used in the discharge and neutralizer cathodes. The cathode tubes consist of a molybdenum-rhenium alloy with a thoriated tungsten orifice plate. The orifice diameters for the discharge and neutralizer cathodes were 1.52 mm and 0.51 mm, respectively. Porous tungsten inserts, impregnated with a low work function compound were used as the emitters.

Testing was conducted with two-grid ion optics using both a standard J-series titanium mounting system (as depicted in Fig. 1) and an all-molybdenum mounting system. The electrodes had a nominal thickness of 0.36 mm, with 1.91 mm and 1.14 mm diameter screen and accelerator apertures, respectively. The open-area-fraction for the screen and accelerator electrodes was 0.67 and 0.24, respectively. The nominal electrode cold-gap was set at 0.66 mm.

Figure 2 shows a power supply circuit diagram for the derated ion thruster which requires only 4 power circuits for steady-state operation, with 2 additional circuits for the discharge and neutralizer cathode heaters used on start-up only. A total of 8 power leads run to the thruster. The derated thruster does not utilize a discharge cathode keeper or starting electrode. Discharge ignition is obtained using open circuit voltage of the discharge supply to initiate the cathode to anode discharge.

Testing was conducted in the tank 5 vacuum chamber facility at Lewis Research Center (LeRC). The chamber is 4.6 m in diameter by 19.2 m in length. The pumping characteristics of the facility include an 88 kℓ/s xenon pumping speed (with oil diffusion pumps), a no-load pressure of < 1.3×10^{-5} Pa, and an operational pressure of < 6.7×10^{-4} Pa. Additional testing to quantify facility-enhanced charge-exchange erosion was conducted with a gaseous helium cryopanel. This panel increased the xenon pumping speed to approximately 130 kℓ/s. Laboratory power supplies[4] were used for thruster performance testing. All tests were performed using research grade xenon propellant. The propellant feed system used was similar to that described in reference 4. Commercial mass flow transducers, calibrated using a primary standard, were used to measure the propellant flow rate to the thruster.

The thruster was operated under manual control for all performance testing. Data were recorded from calibrated digital metering. Steady-state discharge chamber performance curves were obtained under conditions of fixed discharge voltage and fixed beam current. All thruster performance data include a thrust loss which is the product of a beam divergence factor (estimated at 0.98) and a doubly-charged ion factor (estimated from previous charge-state documentation of xenon ion beams). Total efficiency and specific impulse calculations include accelerator drain and neutralizer power, and neutralizer flow rate. No attempts were made to optimize the ion optics or neutralizer design for the derated conditions. All propellant efficiencies include a correction to the mass flow rate for propellant ingested from the facility.

Performance parameters for the derated ion thruster are compared to published information for the smaller NSSK ion thrusters. These comparisons are made at the design input power level of each of the thrusters. These include the MELCO 12 cm divergent-field[5-7] and NAL 14 cm ring-cusp[8], the UK-10/T5 10 cm divergent-field[2,9-12], the RIT10 8.5 cm and RIT15 13.5 cm rf-discharge[1,13-16], and the Hughes 13 cm ring-cusp[17-18] thrusters.

Thruster component erosion estimates, based on analyses and wear-test data, are made to compare relative reliability and risk. Due to the general lack of lifetest information, emphasis is placed on fundamental analyses based on published thruster operating parameters such as electrode voltages and current densities.

Results and Discussion

Performance

Figure 3 shows the demonstrated range of thrust and input power of the 30 cm derated ion thruster. The performance results include: a demonstrated 33:1 power- and thrust-throttling capability, over a 4.5:1 range in specific impulse; a maximum thrust-to-power ratio of 55 mN/kW achieved at 1517 sec specific impulse and 554 W input power; R-ratios from 0.3-to-0.9, demonstrated with 2-grid ion optics at both low and high (up to 6.4 mA/cm^2) ion current densities; and beam voltages as low as 100 volts (obtained at a beam current of 0.4 A).

A plot of thruster efficiency versus specific impulse over the range of 1500-to-3000 seconds is shown in Fig. 4. Increases in thrust over those values indicated in Fig. 4 (for the same specific impulse range) are probably feasible. These preliminary data were obtained at a large electrode gap set for high power operation. At the lower power levels corresponding to the data of Fig. 4, significant improvements in baseline perveance and hence thrust

would be anticipated with a smaller electrode gap.

Figure 5 shows the variation in discharge losses (beam ion production cost) and total discharge power for the derated thruster operating over the input power range of approximately 0.2-6.0 kW. The data of Fig. 5 were obtained at 28 volts discharge voltage and data above 1.9 kW were obtained at 90% discharge chamber propellant efficiency. Below this power level, the fixed neutral loss rate resulted in a decay in discharge chamber propellant efficiency down to a minimum of approximately 80%. As indicated, the discharge losses drop with increasing input power; from a peak of 274 W/A at 310 W to 152 W/A at 6.0 kW. The discharge power increases linearly with input power, going from 100 W to a maximum of 600 W.

As illustrated in Figs. 3 and 4, the derated thruster offers a great flexibility in operating parameters. As a consequence, for a fixed input power to the thruster, a widely varying range of specific impulse and thrust levels are obtainable. This is illustrated in Fig. 6a, where the thrust-to-power ratios of the derated thruster are compared to those of the MELCO[6], NAL[8], UK-10/T5[9], and the RIT15[14] ion thrusters. The thruster data shown were all obtained at the same input power level (640 W +40/-20 W). It can be seen that the derated thruster provides thrust levels up to 80% higher than obtainable with the smaller ion thrusters at the same input power level. This is because the derated thruster operates at higher beam currents than the smaller NSSK thrusters. Note that the UK-10/T5 thrust data are uncorrected for divergence or multiply-charged ions, so that the true thrust-to-power ratio would be somewhat lower than that indicated. A similar conclusion results from comparing the performance of the derated thruster to that of the RIT10[14] and the Hughes 13 cm[18] thrusters, as illustrated in Fig 6b. The data of Fig. 6b were obtained at input power levels of 425 W ± 35 W. The datum for the HRL 13 cm thruster is projected performance. The derated engine thrust levels are as much as 50% higher than that of the RIT10 at the same input power level.

Relevant design and operating parameters for the derated and smaller NSSK thrusters are listed in Tables 1 and 2. The performance parameters identified in Table 1 include those presented in Figs. 6a and 6b. The operating conditions identified for the MELCO thruster are the design point for this thruster.[6] The NAL thruster data were obtained from a recent 1000 hr thruster endurance test.[8] The data for the UK-10/T5, RIT 10, and Hughes thrusters are at the operating conditions proposed for use on the INTELSAT-VII spacecraft.[9,12,16,18] The data for the RIT 15 thruster, at an input power comparable to the MELCO and UK-10/T5 thrusters, were obtained from reference 14. Table 1 also lists data for the derated thruster, at the lowest thrust-to-power ratio. The identified conditions for the derated thruster represent the most conservative performance, and were those used in evaluating relative component erosion. All data of Figs. 6a and 6b for the derated ion thruster were obtained at beam voltages ≤ 560 volts. This is in contrast to the data for the smaller thrusters, obtained at beam voltages in the range of 1000-to-1500 volts.

The primary reason for the difference in performance between the derated thruster and the other thrusters is due to the larger beam area. For a given input power level, the larger beam area permits operation at lower extraction voltages and higher beam currents. This results in higher thrust levels at lower values of specific impulse. The higher thrust levels result in reduced on-orbit thrusting time which, in turn, reduces the ground qualification times.

The reductions in on-orbit thrusting time using the derated thruster approach are illustrated in Fig. 7. The assumptions for Fig. 7 include: an initial spacecraft mass in geosynchronous orbit of 1850 kg (baseline INTELSAT-VII size[19] with ion propulsion option), a mission delta-v of 46 m/s/yr, 1 (single-pair) nodal firing per day, a thruster cant angle of 30 degrees, and a 15 year mission life. The thrust levels for the derated and other thrusters are those of Fig. 6a, obtained at a nominal 640 watts input power. As indicated, the derated thruster requires thruster operating times of order 50-to-75% less than those of the smaller thrusters. The lower specific impulse range of the derated thruster has negligible impact on the total propellant requirement and mass benefit obtainable with the ion propulsion system option.[20] The RIT10 and HRL 13 cm thrusters would require ~ 21,400 and ~ 11,700 hours total thrusting time respectively, for the same mission application.

Component Erosion

This section presents simple analyses to quantify the expected differences between critical component erosion in the derated thruster and in the smaller NSSK thrusters.

One of the primary life limiting erosion mechanisms of the ion thruster is sputter erosion of cathode potential surfaces in the discharge chamber by discharge ions. The sputtered discharge material can deposit on anode surfaces and subsequently result in flakes of spalled material electrically shorting the thruster grids.[21-22] Sputter eroded and deposited material can coat anode and insulator surfaces in the discharge, resulting in changes in surface conductivity which can impact thruster performance and reliability.[22-23] Additionally, the sputter erosion of surfaces can result in structural failure of discharge chamber components.

A unique design feature of the derated ion thruster is that it employs essentially no cathode potential surfaces exposed to the discharge except for the hollow cathode and the screen grid. All other dc-discharge thrusters, including the smaller NSSK thrusters, employ keepers, pole piece surfaces, and baffles, all at cathode potential, in close proximity to the discharge cathode. These surfaces, which are integral to the efficient operation of the other thruster designs, are susceptible to high erosion rates via the 'cathode jet' phenomena[24], observed in several recent tests.[4,24-25] Since the derated ion thruster has few discharge design features in common with the smaller NSSK thrusters except for the cathode potential screen grid electrode, comparisons of relative discharge chamber erosion will be based on this component.

The internal erosion rate of the screen grid is proportional to

$$R_{scrn} \propto \frac{j^{+} \cdot Y(E) + \frac{j^{++}}{2} \cdot Y(2E)}{\phi_s} \qquad (1)$$

where ϕ_s is the screen grid transparency to ions, j^{+} and j^{++} are the singly- and doubly-charged ion current densities with the sum of these two densities equal to the ion beam current density, and $Y(E)$ is the sputter yield due to ion bombardment at energy E. Equation (1) simply states that the erosion rate is given by the product of the ion current density impinging on the screen grid and the physical sputter yield at the incident ion energy, with the doubly-charged ions being accelerated by the sheath drop to twice the energy of the singly-charged ions.

Figure 8 plots the average beam ion current density of the derated thruster and the smaller NSSK ion thrusters versus specific impulse for 620-680 W input power. The average beam ion current density is the beam ion current divided by the beam area. As indicated, the derated ion thruster operates at current densities a factor of ~ 2-to-5 below that of the smaller thrusters.

For this analysis sputtering contributions from both singly- and doubly-charged ions were assumed. As there are no published data for j^{++}/j^{+} available for the smaller NSSK thrusters with xenon propellant, data obtained from a 30 cm ring cusp xenon ion thruster were used to estimate the values for the smaller thrusters. For a fixed thruster geometry, the j^{++}/j^{+} ratio has been shown to be, to first-order, dependent soley on discharge chamber propellant efficiency.[26-27] As the discharge chamber propellant efficiencies for the derated and smaller NSSK thrusters are all in the range of 81-86%, the estimated centerline ratios for the thrusters are therefore comparable (in the range of 2.4-3.7%). Centerline estimates were used as these represent the peak j^{++}/j^{+} current density ratio, corresponding to the location of maximum screen grid erosion.

Data for low energy sputtering (< 100 eV) for xenon ions on molybdenum and other refractory metals is virtually non-existent. However there are many models in the literature which attempt to predict sputtering yields under normally incident ion bombardment at very low energies. One relatively simple relation for low energy sputtering is in the form[28]

$$Y(E) = k \cdot (E - E_{th})^2, \quad \begin{matrix} E_{th} \le E < 10^2\ eV \\ k = const \end{matrix} \qquad (2)$$

where E is the incident ion energy, and E_{th} is the target threshold energy. The constant k was determined by fitting the experimental sputtering datum at the lowest energy (100 eV) for which sputter yield information is available[29], and results in a value of 1.06×10^{-5}. An E_{th} of 24.8 volts for xenon ions on molybdenum, corresponding to 4 times the sublimation energy of the latter, was taken.[28] Assuming a smooth transition from 100 eV to the lower energies, Eq. (2) with these values for the constants should provide a reasonable first order prediction of the sputter yield. A plot of this estimated sputter yield versus energy for xenon ions on molybdenum up to 100 eV is shown in Fig. 9.

The incident energy of singly-charged discharge chamber ions striking the cathode potential screen grid can be approximated by the discharge voltage (doubly-charged ion energies being twice this voltage). Although the controlling physics for the discharge voltage involves several parameters including neutral and plasma densities, an effective anode area, and a magnetic component, it is illustrative to plot the operating discharge voltage versus beam diameter for several ion thrusters. As seen in Fig. 10, an increasing beam diameter in general permits lower operating discharge voltages, for a fixed high propellant efficiency. All data of Fig. 10 were obtained at 90% propellant efficiency, or at a slightly lower value associated with the maximum obtainable efficiencies demonstrated for the smaller thrusters on xenon propellant. Figure 10 also includes xenon data obtained from modified IAPS[30] and SERT II[31] thrusters. As indicated, the derated thruster operates at lower values of discharge voltage in comparison to the smaller NSSK ion thrusters. By using the discharge voltages of Fig. 10 in the sputter yield equation, the sensitivity of the yield to small changes in the discharge voltage is apparent.

Using Eqs.(1) and (2), a relative measure of screen grid erosion rates, can be obtained and is presented in Fig. 11, where the data are normalized to the value obtained for the derated thruster. As shown, the relative erosion rates of the

screen grid for the smaller thrusters are 16-to-90 times that for the derated ion thruster. This is due to the combination of lower ion current density and discharge voltage of the derated ion thruster. For all the data of Fig. 11 except the UK-10 thruster, a value of 0.8 was used for the transparency of the screen grid to ions, which is typical of 30 cm high perveance ion optics. For the UK-10 thruster, a value of 0.9 was used.[12] The analysis indicates that the dominant sputtering agent for the derated ion thruster is Xe^{++} (~ 1.7:1), while that of the smaller NSSK thrusters is Xe^{+} (~ 3.0 - 6.7:1).

Although there are insufficient experimental data to compare measured screen grid erosion rates among the thrusters identified in Fig. 11., there are lifetest data which qualitatively support the estimated order-of-magnitude differences. For example, recent thruster lifetests have been completed including a 1000 hour test of the NAL thruster[8] (at the conditions identified in Tables 1 and 2), and a 900 hour test of a 30 cm ion thruster at 5.5 kW input power.[4] The design of the 30 cm thruster was comparable to that of the derated ion thruster shown in Fig. 1. It was operated at a current density of 5.11 mA/cm^2, a discharge voltage of 26.9 volts, and a j^{++}/j^{+} ratio of 0.06. Although the 30 cm thruster was operated at a higher current density than the NAL thruster (a factor of 4 higher than that of the derated thruster operated at 644 W), the 30 cm thruster showed a significantly lower discharge chamber erosion rate, with negligible deposition and no spalling. The NAL thruster, on the other hand, experienced much deposit spalling and large flake formation. This difference in internal erosion rates is attributable to the difference in operating discharge voltage. The analysis for Fig. 11 may indeed be somewhat conservative, as there are data supporting a higher value of E_{th}. For example, reference 32 gives a value of 27 eV. Using this value in the analysis would increase the indicated relative erosion rates by as much as 45%.

It should be noted that reductions in the discharge chamber component erosion rates may be obtained by using alternative materials or surface coatings. However, modification of the screen grid material would not be expected to have more than a factor of 2.5 impact in reducing the erosion rate.[33] Additionally, by modifying the screen grid potential (such as by permitting it to float) one might anticipate a reduction in grid erosion, a technique that could be employed with all thrusters. However this does not address erosion of other cathode potential surfaces in the discharge chamber.

A potentially more serious life-limiting phenomena of the ion thruster is charge-exchange erosion of the accelerator grid. This erosion impacts thruster lifetime, and results in metal efflux from the thruster which can coat spacecraft surfaces. Charge-exchange ions are created when the 'slow ' unionized propellant atoms emitted from the thruster undergo a resonance charge-transfer with the 'fast' energetic beam ions. Under certain conditions, the charge-exchange ion can be focussed back onto the negatively charged accelerator grid, causing sputtering of the downstream grid surface and forming the characteristic pits on the webbing between adjacent grid holes. Over a prolonged period of time the erosion can lead to structural failure of the accelerator grid.

The charge-exchange ion erosion rate of the accelerator grid is proportional to

$$R_{accel} \propto \sigma_{c\text{-}x} \cdot j_b \cdot j^0 \cdot Y(E) \qquad (3)$$

where $\sigma_{c\text{-}x}$ is the resonance charge-exchange cross-section for xenon, and j_b and j^0 are the beam ion current and neutral densities respectively. An additional term for the effective charge-exchange length is assumed constant for all thrusters. Experimental verification for this assumption is not available but it is felt to be appropriate for the order of accuracy of the calculations herein. Charge-exchange cross-section data for xenon are fairly well known over the energy range of interest. Cross-section data and calculations from references 34 and 35 are shown in Fig. 12. For this analysis, the data of reference 35 were used.

The average neutral density term in Eq. (3) is the neutral loss rate divided by the beam area. The average neutral density values for the various thrusters are shown in Table 2, ranging from approximately 0.2 mA/cm^2 for the derated thruster, to as high as 1.0 mA/cm^2 for the MELCO and UK10/T5 thrusters.

The sputter yields for xenon ions on molybdenum have been experimentally determined for energies ≥ 100 eV. Figure 13 shows sputtering data over the range of 100-to-800 eV from references 29 and 36. The data from reference 29 fit the quadratic equation

$$Y(E) \approx -0.187 + 2.515^{-3}(E) - 7.298^{-7}(E)^2 \quad \text{for } 100\ eV \le E \le 800\ eV. \qquad (4)$$

The incident energy of the charge-exchange ions can be approximated by the accelerator grid voltage. Since the derated thruster has a larger beam area, it is capable of operating at lower total accelerating voltages than the smaller NSSK thrusters, for a fixed input power. This in turn means a lower accelerator grid voltage. Table 2 lists the accelerator grid voltages of the derated and NSSK thrusters at each of the respective design points.

Using Eq. (3) and (4), and the data of Figs. 12 and 13,

relative accelerator grid erosion rates can be obtained. These are presented in Fig. 14, where the data are normalized to the value obtained for the derated thruster. As indicated in Fig. 14, the normalized erosion rates of the smaller thrusters range from ~ 40-to-70 times higher than that of the derated ion thruster. A total efflux parameter, a relative measure of the sputtered metal removed from the accelerator grid over its operational life, may be calculated from the product of the normalized accelerator grid erosion rate, the beam area, and the required thrusting time identified in Fig. 7. Such calculations predict factors of ~ 10-to-20 times greater accelerator grid efflux from the smaller thrusters, as compared to the derated ion thruster.

There are options available to mitigate the metal efflux from the thruster. These include the use of plume shields and/or 3-grid ion optics. Plume shields do not reduce the magnitude of the electrode erosion. Three grid optics may impact erosion rates, although in early tests it was found that the overall mass loss rates did not decrease with xenon. Additionally, with 3-grid optics the charge-exchange ions are focussed onto the walls of the accelerator grid apertures, which results in a continually increasing neutral loss rate and degradation in thruster performance with time.[37] Both of these approaches add mass and complexity to the thruster.

Under normal operating conditions most of the accelerator drain current is due to charge-exchange ion impingement. By equating the measured accelerator current to charge-exchange ion current and multiplying by the appropriate sputter yield, it is possible to correlate this product to measured accelerator grid mass loss rates. This correlation is shown in Fig. 15, where the measured accelerator grid mass loss rates from several wear-tests with molybdenum grids are plotted versus the product of the accelerator grid drain current and the sputter yield. The data of Fig. 15 includes test results for both xenon and mercury propellant ion thrusters, with both 2- and 3-grid ion optics.[4,8,23,37-38] Figure 15 indicates that estimates of accelerator grid mass loss rates can be made with reasonable accuracy from the measured drain currents.

In the most recent wear-tests of xenon ion thrusters, the charge-exchange erosion of the accelerator grid appeared to be the most serious and fundamental limitation to thruster lifetime, especially at higher power levels.[4,39] Under these test conditions the charge-exchange ion current impinging on the accelerator grid has been shown to be, to first-order, a function of the facility pressure. Therefore, a dominant term in the volume ion production of charge-exchange ions is the neutral density contribution due to residual propellant atoms in the facility.

The minimum pumping speed requirement of an ion thruster lifetest facility can be quantified as a function of test duration and thruster operating condition. That is, if the accelerator grid impingement current is 'facility-enhanced', a minimum pumping speed can be quantified which is necessary to reduce the charge-exchange erosion over the lifetest duration to an acceptable level.

As previously shown, if the impingement current and thruster operating condition are known, a mass loss rate of the accelerator grid can be estimated. It is then necessary to estimate a maximum acceptable mass loss rate. This can be done by equating the mass loss rate to an etch rate. As an example, a conservative estimate of end-of-life for the accelerator grid could be the erosion of the charge-exchange trenches (the region between the pits) to a depth equal to half the thickness of the original electrode. Based on post-lifetest analyses of accelerator grids, it is estimated that the maximum acceptable mass loss for a 30 cm diameter molybdenum electrode of 0.38 mm thickness would be ~ 36 gm. This defines then a maximum acceptable impingement current, at the fixed thruster accelerator grid voltage, for a given length lifetest.

It is then necessary to know the sensitivity of the impingement current to facility pressure at the fixed thruster operating condition. Figure 16 shows this variation for fixed operating points of the thruster. The data of Fig. 16 were obtained by increasing the facility pumping speed using a helium cryopanel and noting the change in impingement current with decreasing facility pressure. Once this sensitivity is known, a maximum acceptable facility pressure can be identified from the maximum acceptable grid erosion rate. Since the gas throughput and pressure are known, a minimum pumping speed can then be defined.

Figure 17 shows the estimated minimum pumping speed as a function of thruster input power for 5000 and 10,000 hr lifetests of a derated thruster. The minimum pumping speed is that which is necessary to insure that 'facility-enhanced' charge-exchange erosion is sufficiently low to preclude reaching accelerator grid end-of-life prior to lifetest completion, according to the above mass-loss criterion. A 30 cm diameter molybdenum accelerator grid electrode of 0.38 mm thickness is assumed. The figure indicates that for thruster input power levels of $\leq$ 1500 W, corresponding to a maximum mass flow rate of approximately 1.8 A eq. xenon, pumping speeds of $\leq$ 30 kℓ/s are sufficient to meet the accelerator grid erosion limitation.

Growth Potential

In addition to the previously mentioned performance characteristics, the derated thruster is capable with little modification of operating at substantially higher power.

This allows the same thruster design to be implemented as user requirements increase. This growth potential, inherent in the derated design, is shown in Fig. 18, a plot of thrust versus input power. As indicated, a linear increase in thrust, from approximately 30-to-80 mN, is obtained over the input power range of 0.6-to-1.6 kW. Additionally, as indicated in Fig. 3, the derated thruster is capable of operating at power and thrust levels of 6 kW and 250 mN, respectively, which are conditions appropriate to primary propulsion functions.

The impact of this potential for NSSK applications is shown in Fig. 19, where the required thruster operating time versus thruster input power is plotted for a 15 year mission of a 2000 kg spacecraft (comparable to a growth-version INTELSAT VII[19] with ion propulsion option). The other mission parameters are as previously defined. The figure shows that the thrusting time is reduced to less than 3200 hours per thruster for input power levels above about 1400 W.

Integration

Although the derated thruster has significant performance and lifetime advantages over the smaller NSSK ion thrusters, its relatively large mass and volume raise spacecraft integration concerns. The laboratory version derated thruster depicted in Fig. 1 has a mass of approximately 10.7 kg, including cable harness and ground screen. This mass is considerably greater than the values quoted for the smaller thrusters, as indicated in Table 1. Care should be taken in interpreting the thruster masses however. The available mass data for the smaller thrusters appear to be both measurements and estimates. Additionally some mass data include elements such as propellant mass flow control devices, gimbals and thruster mounting structure while others do not.

An optimization program is underway to reduce the mass of the derated thruster to < 7.0 kg for an engineering model version. Redesign of the magnetic circuit and a reduced volume concept appears to make this feasible. The cylindrical-geometry laboratory version thruster is approximately 40 cm in diameter by 36 cm in length. A redesigned version with reduced volume is depicted in Fig 20. A volume reduction of up to 40% is achievable using this approach. This conic geometry has been tested and the redesign has had no detrimental impact on discharge or thruster performance.

Conclusions

A program was initiated to evaluate the impact on operations and critical component erosion of using a derated ion thruster for NSSK propulsion, the results of which are summarized in Table 3. Experimental data were obtained using a 30 cm xenon ion thruster operating at highly-throttled conditions, at low specific impulse and high thrust-to-power ratio. Performance data were obtained over a 33:1 power- and thrust-throttling range, and a 4.5:1 range in specific impulse. Demonstrated thrust levels for the derated thruster were as much as 80% more than for the smaller NSSK ion thrusters, for the same input power levels. The higher thrust levels offer the advantage of reduced on-orbit thrusting time, which in turn reduces the ground qualification time.

Thruster life and reliability are enhanced in the derated thruster because it operates at lower ion current densities and lower discharge and accelerating voltages. This results in lower internal and external component erosion rates, and reduction of metal efflux from the thruster. The derated ion thruster screen and accelerator grid erosion rates are estimated to be at least 16 and 41 times lower than those of the smaller NSSK thrusters operating at the same input power level. Total metal efflux from the accelerator grid is estimated to be 10-to-20 times lower over the required operational life. Minimum pumping speed requirements to reduce 'facility-enhanced' charge-exchange erosion of the accelerator grid to acceptable limits were quantified. Pumping speeds ≤ 30 kℓ/s are predicted to be sufficient for a 10 khr lifetest of a derated ion thruster at NSSK-type power levels.

With little modification, the derated thruster is capable of operating at substantially higher input power levels than that projected for the baseline NSSK mission. This allows the same thruster to be employed for more demanding user requirements, whether these be for NSSK or primary propulsion applications. Total on-orbit thrusting times of < 3200 hours per thruster (at 1400 W per thruster) are projected for 15 year stationkeeping missions on 2000 kg-class spacecraft. Redesign of the derated thruster has reduced its volume by up to 40% and is expected to reduce its mass by 30%, with no effect on its performance. These reductions should facilitate spacecraft integration of the thruster.

Acknowledgements

Thruster fabrication and assembly services provided by George Jacynycz, Craig Nelson, Carl Ollick, and Eugene Pleban are gratefully acknowledged.

References

[1]Groh, K., et. al., "Development Status of the RIT Ion Engines," AIAA Paper No. 90-2671, July 1990.

[2]Fearn, D.G., "The Proposed Demonstration of the UK-10 Ion Propulsion System on ESA's SAT-2 Spacecraft," AIAA Paper No. 88-031, October 1988.

[3]Kajiwara, K. and Katada, M., "Test Facilities for the ETS-VI Ion Engine System," AIAA Paper No. 90-2656, July 1990.

[4]Patterson, M.J. and Verhey, T.R., "5kW Xenon Ion Thruster Lifetest," AIAA Paper No. 90-2543, July 1990.

[5]"Engineering Test Satellite-VI (ETS-VI) Xenon Ion Engineering System (XIES)," Mitsubishi Electric Corporation, TL9-88-094, March 1988.

[6]Shimada, S., et. al., "Ion Engine System Development of ETS-VI," AIAA Paper No. 89-2267, July 1989.

[7]Personal communication, P.J. Wilbur, Colorado State University, August 1990.

[8]Kitamura, S., Miyazaki, K., and Hayakawa, Y., "1000 Hour Test of 14 cm Diameter Ring-Cusp Xenon Ion Thruster," AIAA Paper No. 90-2542, July 1990.

[9]Smith, P., "Design and Development of the UK-10 Ion Propulsion Subsystem," AIAA Paper No. 88-033, October 1988.

[10]Fearn, D.G., Martin, A.R., and Smith, P., "Ion Propulsion Research and Development in the UK," IAF Paper No. 89-274, October 1989.

[11]Mohan, M. and Wallace, N.C., "Integration of a Power Conditioning and Control System with the T5 Ion Thruster," AIAA Paper No. 90-2630, July 1990.

[12]Fearn, D.G., "The UK-10 Ion Propulsion System Status and Applications," presented at the INTELSAT Symposium on Ion Propulsion for Communication Satellites, July 1989.

[13]Groh, K.H., et. al., "Auxiliary Propulsion RF-Engine RIT 15 - Prototype Design and Performance," AIAA Paper No. 88-034, October 1988.

[14]Bassner, H., et. al., "Recent Developments of the North-South-Stationkeeping Engines of the RIT-Family," IAF Paper No. 89-273, October 1989.

[15]Bassner, H., Berg, H.P., and Kukies, R., "The Design of RITA Electric Propulsion System for Sat 2 (Artemis)," AIAA Paper No. 90-2539, July 1990.

[16]Bassner, H., "RF-Ion Thruster Assembly RITA," presented at the INTELSAT Symposium on Ion Propulsion for Communication Satellites, July 1989.

[17]Beattie, J.R. and Penn, J.P., "Electric Propulsion - A National Capability," AIAA Paper No. 89-2490, July 1989.

[18]Beattie, J.R., "Status of Xenon Ion Propulsion Technology for Stationkeeping," presented at the INTELSAT Symposium on Ion Propulsion for Communication Satellites, July 1989.

[19]Day, M.L., et. al., "INTELSAT VII Ion Propulsion Subsystem Implementation Study," AIAA Paper No. 90-2550, July 1990.

[20]Rawlin, V.K. and Majcher, G., "Mass Comparison of Electric Propulsion Systems for NSSK of Geosynchronous Spacecraft," AIAA Paper No. 91-2347, June 1991.

[21]Nakanishi, S. and Finke, R.C., "A 9700-Hour Durability Test of a Five Centimeter Diameter Ion Thruster," AIAA Paper No. 73-1111, October 1973.

[22]Collett, C.R. and Poeschel, R.L., "A 10,000 Hour Endurance Test of a 700 Series 30-cm Engineering Model Thruster," AIAA Paper No. 76-1019, November 1976.

[23]Power, J. L., "Sputter Erosion and Deposition in the Discharge Chamber of a Small Mercury Ion Thruster," AIAA Paper No. 73-1109, October 1973.

[24]Brophy, J.R. and Garner, C.E., "Tests of High Current Hollow Cathodes for Ion Engines," AIAA Paper No. 88-2913, July 1988.

[25]Brophy, J.R. and Garner, C.E., "A 5,000 Hour Xenon Hollow Cathode Life Test," AIAA Paper No. 91-2122, June 1991.

[26]Poeschel, R.L., "2.5 KW Advanced Technology Ion Thruster," Hughes Research Laboratories, Malibu, CA, NASA CR-135076, April 1976.

[27]Rawlin, V.K., "Operation of the J-Series Thruster Using Inert Gas," NASA TM 82977, November 1982.

[28]Wilhelm, H.E., "Quantum Statistical Analysis of Surface Sputtering," *J. Spacecraft and Rockets*, Vol. 13, No. 2, February 1976, pp. 116-118.

[29]Rosenberg, D., and Wehner, G.K., "Sputtering Yields for Low Energy He^+-, Kr^+-, and Xe^+-Ion Bombardment," *J. Applied Physics*, Vol. 33, No. 5, 1962.

[30]Personal communication, Beattie, J.R., Hughes Research Laboratories, August 1990.

[31]Personal communication, Brophy, J.R., Jet Propulsion Laboratory, August 1990.

[32]Stuart, R.V., and Wehner, G.K., "Sputtering Yields at Very Low Bombarding Ion Energies," *J. Applied Physics*, Vol. 33, No. 7, 1962.

[33]Beattie, J.R., "A Model for Predicting the Wearout Lifetime of the LeRC/Hughes 30-cm Mercury Ion Thruster," AIAA Paper No. 79-2079, October 1979.

[34]Dillon, J.A., et. al., "Charge Transfer Reactions in Monatomic and Diatomic Gases," *J. Chemical Physics*, Vol. 23, No. 5, 1955.

[35]Rapp, D. and Francis, W.E., "Charge Exchange between Gaseous Ions and Atoms," *J. Chemical Physics*, Vol. 37, No. 11, 1962.

[36]Weijsenfeld, C.H. and Hoogendoorn, A., "Cathode Sputtering by Rare Gas Ions of Low Energy," in *Ionization Phenomena in Gases*, Vol. I, North-Holland Publishing Company, 1962.

[37]Beattie, J.R., and Matossian, J.N., "Xenon Ion Propulsion for Stationkeeping and Orbit Raising," AIAA

Paper No. 88-052, October 1988.

[38]Nakanishi, S., "A 15,000-hour Cyclic Endurance Test of an 8-cm Diameter Mercury Bombardment Ion Thruster," AIAA Paper No. 76-1022, November 1976.

[39]Rawlin, V.K., "Internal Erosion Rates of a 10-kW Xenon Ion Thruster," AIAA Paper No. 88-2192, July 1988.

Table 1 Design and Performance Parameters for Several Thrusters

Thruster	Design Parameter		Performance Parameter		
	Beam Dia. (cm)	Mass (kg)	Input Power (W)	Thrust (mN)	Isp (s)
MELCO	12.0	3.7	620	23.3	2906
NAL	14.0	a	610	24	3051
UK10/T5[b]	10.0	1.0	644	25	3486
RIT10	8.5	1.5	460	15	3435
RIT15	13.5	2.5	680	20	3575
HRL 13cm[c]	13.0	5.0	427	17.7	2718
DERATED[d]	28.2	10.7[e]	644	30	2285
			451	21	1961

[a]Data not available.
[b]Data are uncorrected for beam divergence or multiply-charged ions.
[c]Projected performance.
[d]Selected data at the lowest thrust-to-power ratio only.
[e]Laboratory-model thruster demonstrated mass; engineering model thruster mass projection < 7.0 kg.

Table 2 Operating Parameters for Several Thrusters

Thruster	Operating Parameter							
	Disch Voltage (V)	Accel Voltage (V)	Beam Voltage (V)	Screen Grid Ion Trans. (Φ_s)	Disch Propel Eff (η_{md})	Grid j_b (mA/cm^2)	Grid j^e (mA/cm^2)	Est'd. j^-/j^+ (%)
MELCO	37.0	496	1000	0.8	0.81	4.25	1.01	2.4
NAL	36.3	800	1021	0.8	0.86	3.03	0.49	3.7
UK10/T5	47.0	350	1100	0.9	0.85	5.82	1.03	3.0
RIT10	a	b	1500	b	b	4.16	b	b
RIT15	a	b	1500	b	b	2.15	b	b
HRL 13cm	28.0[c]	b	b	b	b	b	b	b
DERATED P = 644 W	27.9	141	556	0.8	0.84	1.26	0.23	3.2
DERATED P = 451 W	28.7	120	486	0.8	0.83	0.93	0.20	2.7

[a]Not applicable with rf discharge.
[b]Data not available.
[c]Projected performance.

Table 3 Characteristics of the Derated Thruster Approach

Area	Description	Impact
Performance	higher thrust-to-power ratio	reduced on-orbit thrusting time
		reduced ground qualification time
	flexibility	broad range of available T/P and Isp
Lifetime	permits operation at lower current densities	lower internal and external component erosion
	permits operation at lower internal and external electrode voltages	lower internal and external component erosion
	reduced metal efflux	reduced spacecraft contamination
Growth	thruster capable of higher power operation	negligible redesign required to meet more demanding NSSK requirements
		design useful for primary propulsion
Integration	larger thruster mass and volume	more complex mechanical interface

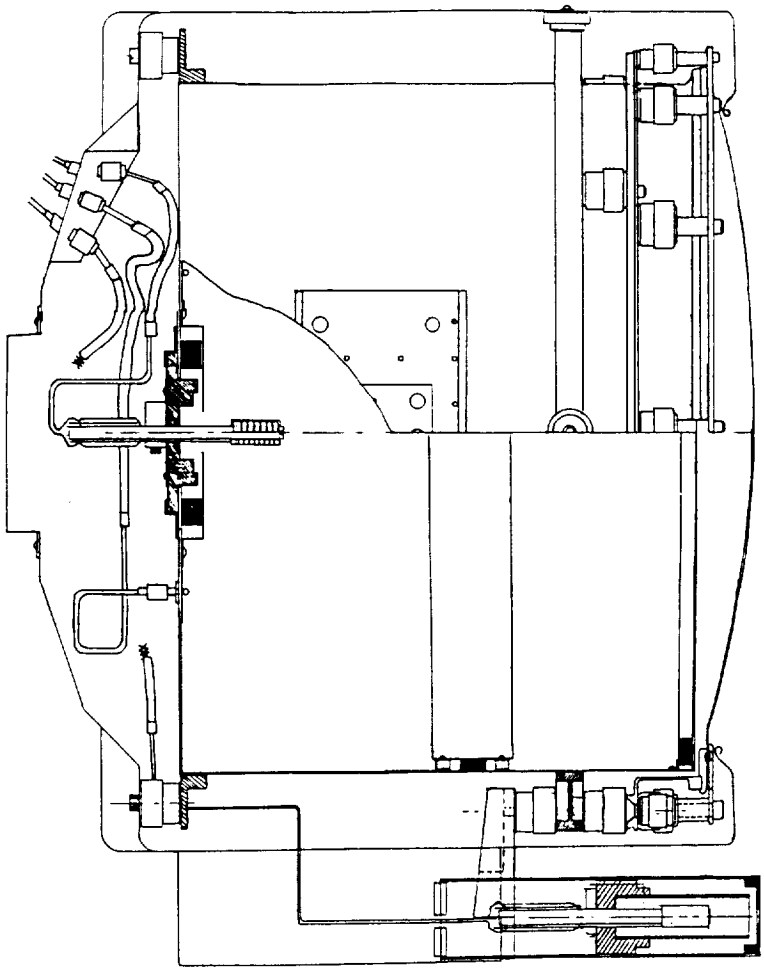

Fig. 1 Cutaway drawing of the 30 cm derated ion thruster.

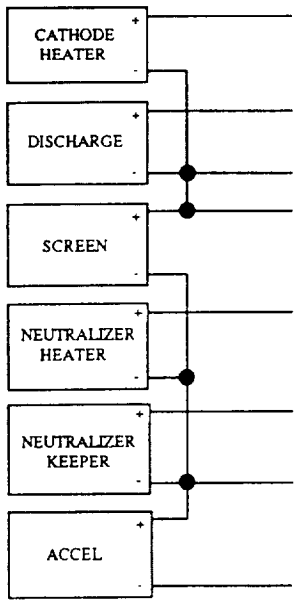

Fig. 2 Power supply circuit diagram for the derated ion thruster.

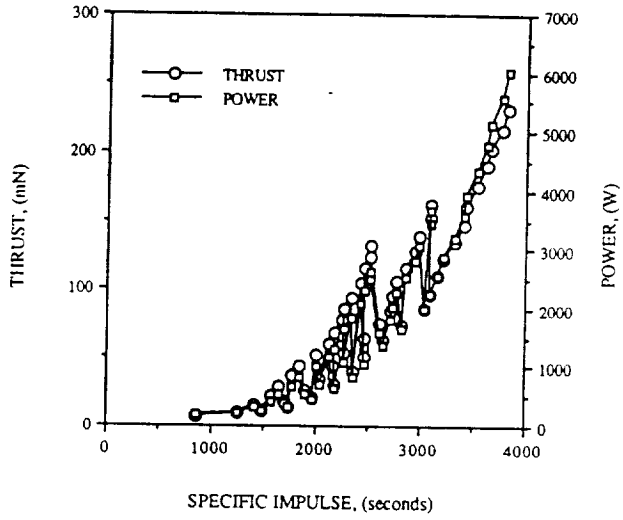

Fig. 3 Demonstrated thrust and input power range of the derated ion thruster.

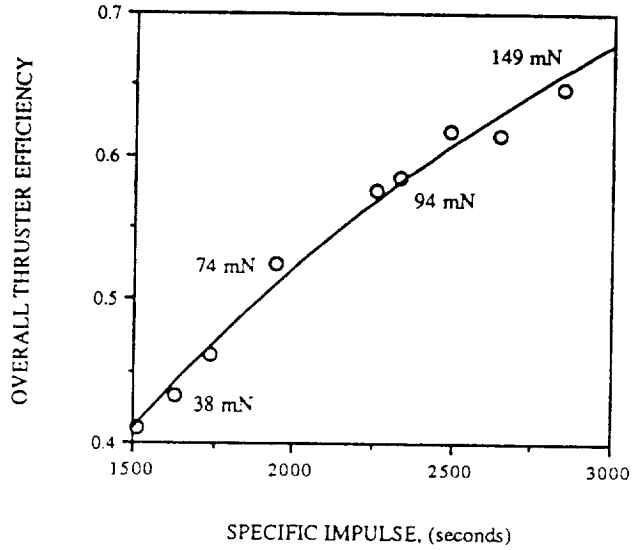

Fig. 4 Thruster efficiency data over the 1500 to 3000 s Isp range; thrust levels are indicated.

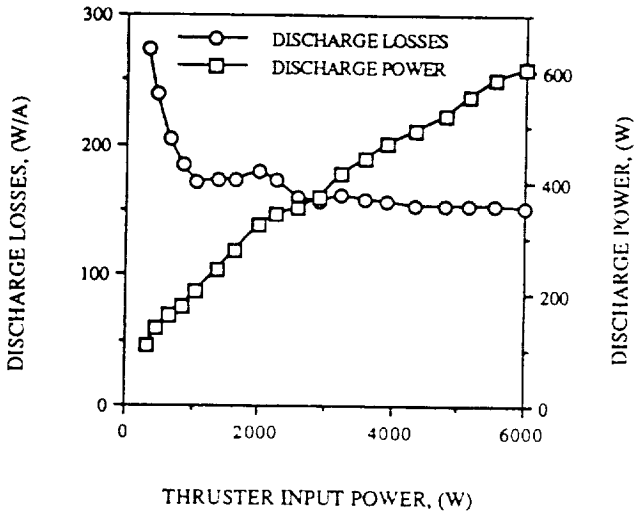

Fig. 5 Variation in discharge losses and total discharge power with thruster input power.

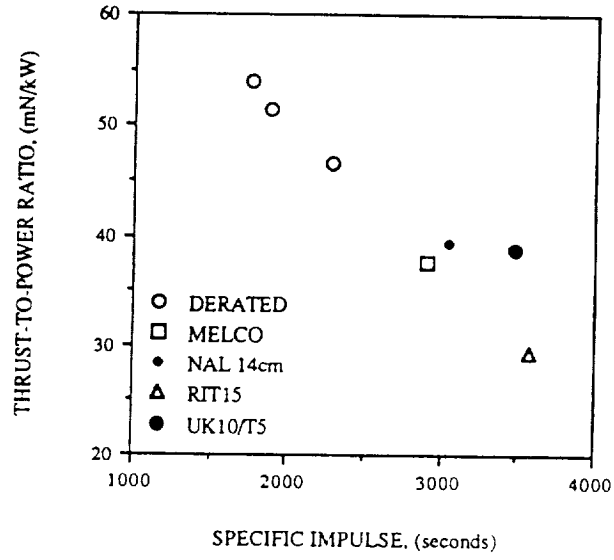

Fig. 6a Comparison of demonstrated thrust-to-power ratios; nominal 640 W input power.

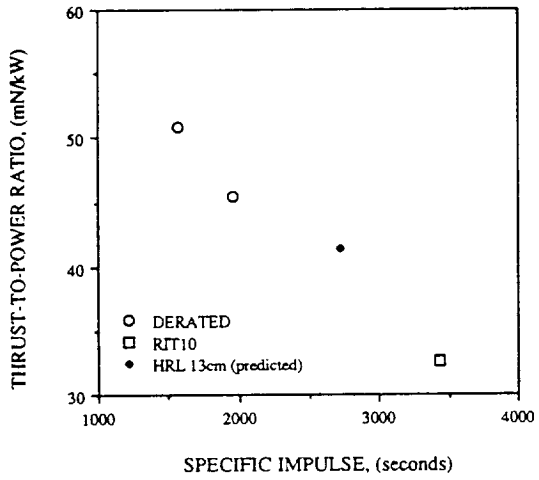

Fig. 6b Comparison of demonstrated thrust-to-power ratios; nominal 425 W input power.

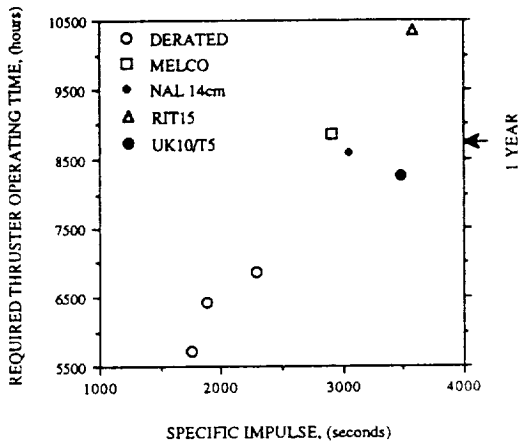

Fig. 7 Comparison of required thrusting times for 15 year stationkeeping of an 1850 kg geosynchronous satellite.

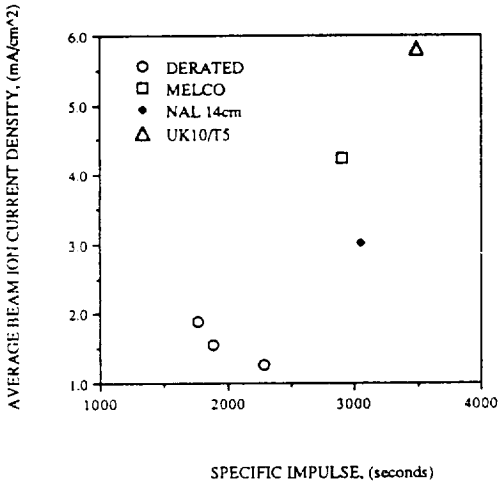

Fig. 8 Comparison of average beam ion current density.

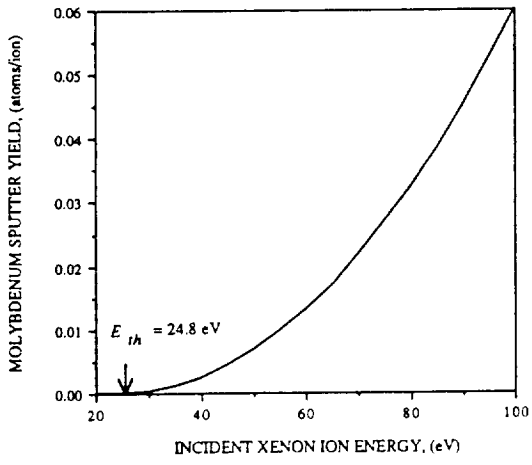

Fig. 9 Estimated sputter yield vs. energy for xenon ions on molybdenum, from Eq. (2).

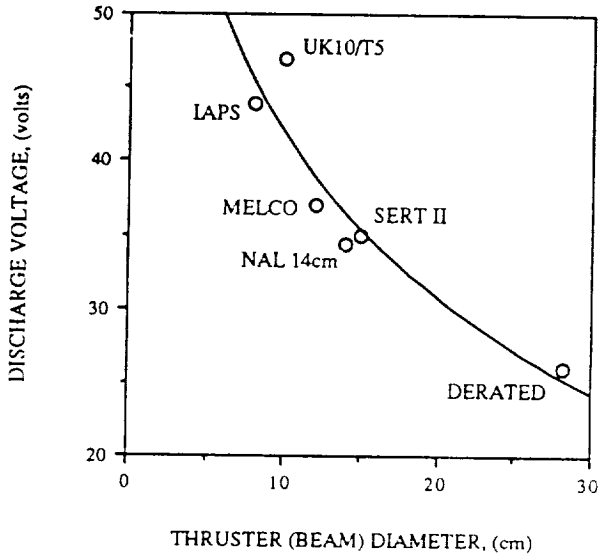

Fig. 10 Discharge voltage for several thrusters vs. beam diameter; data obtained at 90 % propellant efficiency, or maximum on xenon propellant.

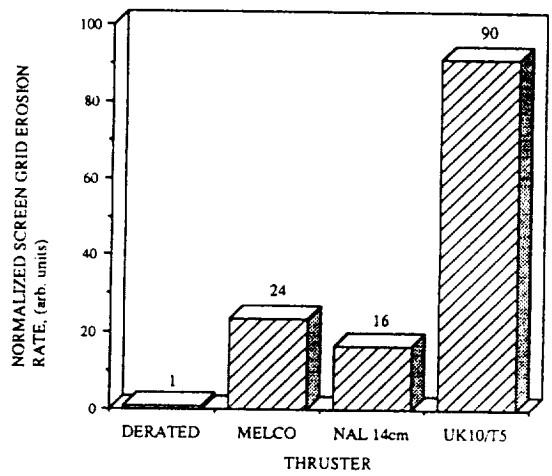

Fig. 11 Normalized screen grid erosion rates, from Eq. (1).

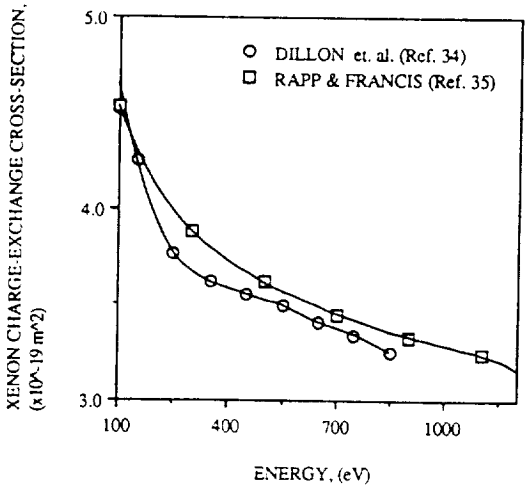

Fig. 12 Resonance charge-exchange cross-section data for xenon.

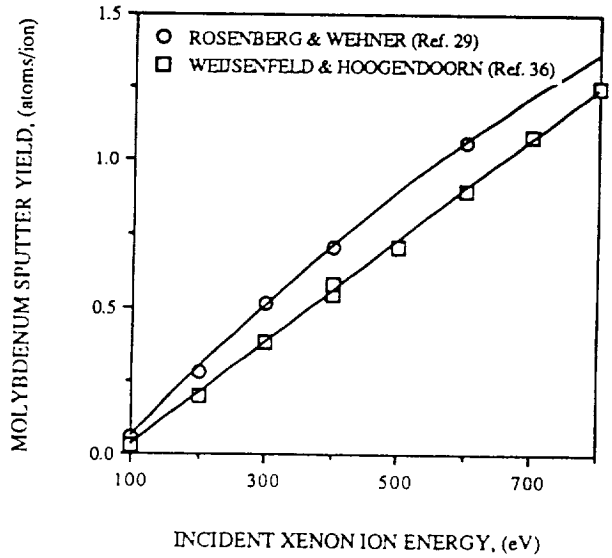

Fig. 13 Sputter yield data vs. energy for xenon ions on molybdenum.

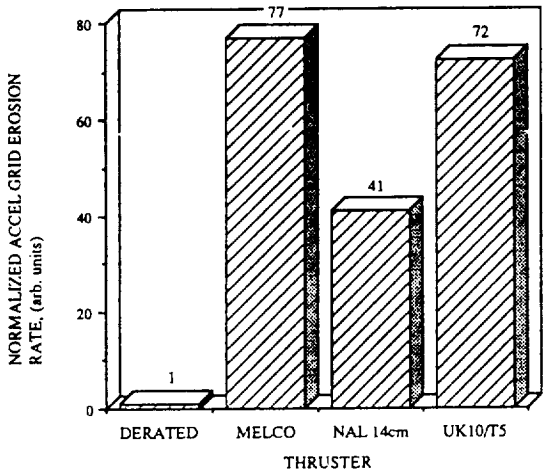

Fig. 14 Normalized accelerator grid erosion rates, from Eq. (3).

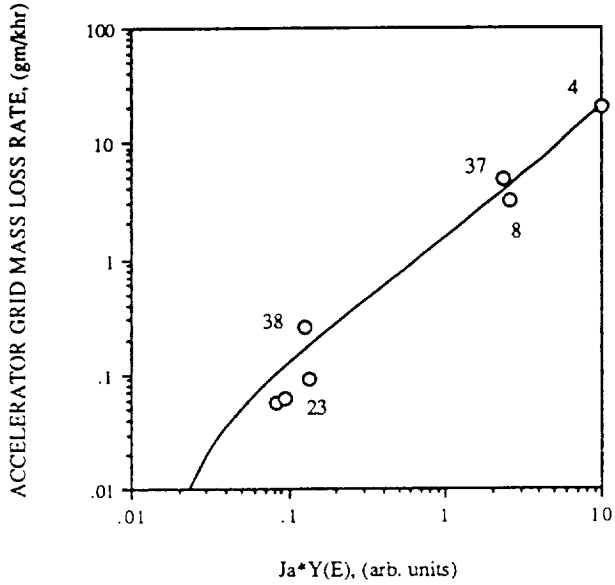

Fig. 15 Accelerator grid mass loss rate correlation; reference numbers are indicated.

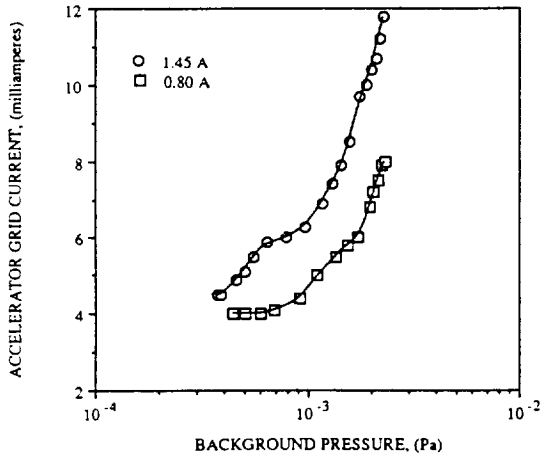

Fig. 16 Sensitivity of accelerator grid impingement current to facility pressure for two values of beam current.

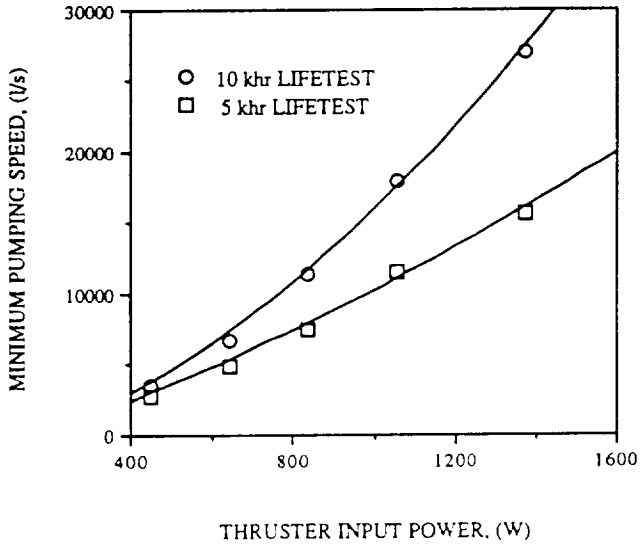

Fig. 17 Estimated minimum pumping speed requirement vs. thruster input power for 5- and 10-khr lifetests of a 30 cm derated ion thruster.

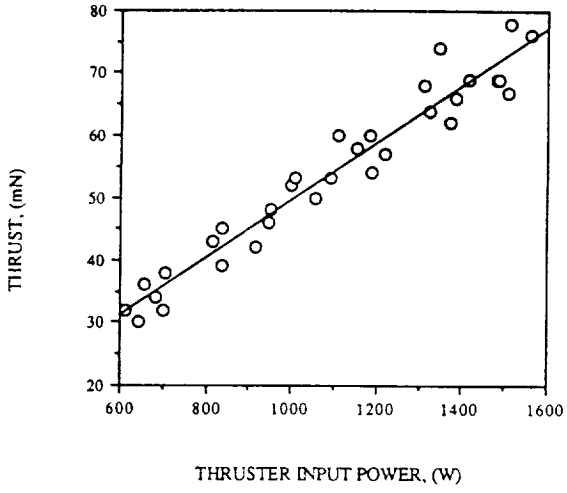

Fig. 18 Demonstrated thrust vs. input power for the derated ion thruster.

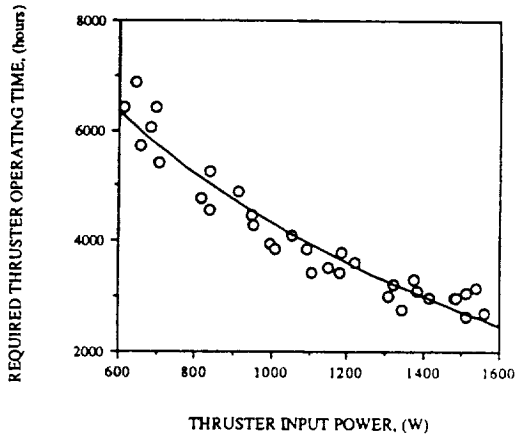

Fig. 19 Required thrusting time vs. input power; 15 year stationkeeping of a 2000 kg geosynchronous satellite assumed.

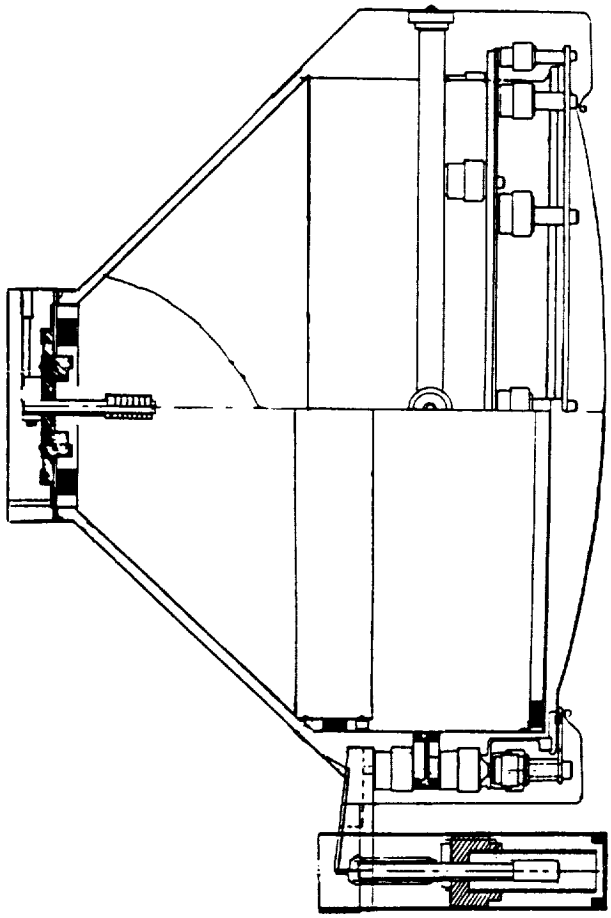

Fig. 20 Cutaway drawing of conic 30 cm derated ion thruster.

NASA
National Aeronautics and Space Administration

Report Documentation Page

1. Report No.	2. Government Accession No.	3. Recipient's Catalog No.
NASA TM-105144 AIAA-91-2350		

4. Title and Subtitle
Performance and Optimization of a "Derated" Ion Thruster for Auxiliary Performance

5. Report Date

6. Performing Organization Code

7. Author(s)
Michael J. Patterson and John E. Foster

8. Performing Organization Report No.
E-6419

10. Work Unit No.
506-42-31

9. Performing Organization Name and Address
National Aeronautics and Space Administration
Lewis Research Center
Cleveland, Ohio 44135-3191

11. Contract or Grant No.

13. Type of Report and Period Covered
Technical Memorandum

12. Sponsoring Agency Name and Address
National Aeronautics and Space Administration
Washington, D.C. 20546-0001

14. Sponsoring Agency Code

15. Supplementary Notes
Prepared for the 27th Joint Propulsion Conference cosponsored by the AIAA, SAE, ASME and ASEE, Sacramento, California, June 24-27, 1991. Michael J. Patterson, NASA Lewis Research Center. John E. Foster, Department of Physics and Atmospheric Sciences, Jackson State University, Jackson, Mississippi 39217. Responsible person, Michael J. Patterson, (216) 433-2405.

16. Abstract
This paper discusses the characteristics and implications of use of a derated ion thruster for north-south-stationkeeping (NSSK) propulsion. A derated thruster is a 30 cm diameter primary propulsion ion thruster operated at highly throttled conditions appropriate to NSSK functions. The performance characteristics of a 30 cm ion thruster are presented, emphasizing throttled operation at low specific impulse and high thrust-to-power ratio. Performance data and component erosion are compared to other NSSK ion thrusters. Operations benefits derived from the performance advantages of the derated approach are examined assuming an INTELSAT VII-type spacecraft. Minimum ground test facility pumping capabilities required to maintain facility enhanced accelerator grid erosion at acceptable levels in a lifetest are quantified as a function of thruster operating condition. Novel approaches to reducing the derated thruster mass and volume are also discussed.

17. Key Words (Suggested by Author(s))	18. Distribution Statement
Ion propulsion Electric propulsion Auxiliary propulsion	Unclassified - Unlimited Subject Category 20

19. Security Classif. (of the report)	20. Security Classif. (of this page)	21. No. of pages	22. Price*
Unclassified	Unclassified	18	A03

NASA FORM 1626 OCT 86

*For sale by the National Technical Information Service, Springfield, Virginia 22161